HHS Public Access

Author manuscript

Chem Catal. Author manuscript; available in PMC 2023 October 20.

Published in final edited form as:

Chem Catal. 2022 October 20; 2(10): 2691–2703. doi:10.1016/j.checat.2022.09.018.

Multiscale simulation-guided design of enzyme bioconjugates with enhanced catalysis

Xiao Hong[1,#], **Timothy Cholko**[2,#], **Chia-en A. Chang**[2,*], **Ian Wheeldon**[3,4,*,&]

[1]Department of Biochemistry, University of California-Riverside, Riverside, CA, 92521

[2]Department of Chemistry, University of California-Riverside, Riverside, CA, 92521

[3]Department of Chemical and Environmental Engineering, University of California-Riverside, Riverside, CA, 92521

[4]Center for Industrial Biotechnology, University of California-Riverside, Riverside, CA, 92521

Summary

Biopolymer-scaffold modification is widely used to enhance enzyme catalysis. A central challenge is predicting the effects of scaffold position on enzyme properties. Here, we use a computational-experimental approach to develop a model for the effects of DNA scaffold position on enzyme kinetics. Using phosphotriesterase modified with a 20bp dsDNA, we demonstrate that conjugation position is as important as the scaffold's chemistry and structure. Multiscale simulations predict the effective substrate concentration increases close to the scaffold, which has μM-strength binding to the substrate. Kinetic analysis shows that the effective concentration that the scaffold provides is best utilized when positioned next to, but not blocking, the active site. At ~5Å distance between scaffold and active site a 7-fold increase in k_{cat}/K_M was achieved. A model that accounts for the substrate concentration as well PTE-DNA geometry accurately captures the kinetic enhancements, enabling prediction of the effect across a range of DNA positions.

eTOC blurb

Biopolymer scaffolds are widely used to enhance enzyme catalysis. Here, we use a computational-experimental approach to define rules for designing enzyme-DNA complexes with enhanced kinetics. Multiscale simulations determined the effective concentration around a DNA scaffold, which exhibits μM-affinity binding to the substrate. This concentration profile along with structural parameters of the enzyme are used as input to a biophysical model. Experimental kinetic

*To whom correspondence may be addressed. wheeldon@ucr.edu, chiaenc@ucr.edu.
#These authors contributed equally to this work
&The lead contact

Author Contributions

All authors conceived the study, designed the research, analyzed the data, and wrote and edited the manuscript. X.H. conducted the experimental analyses; T.C. conducted the simulation and modeling calculations; X.H. and T.C. contributed equally to this work.

Declaration of Interests

The authors declare no competing interests.

analysis of a series of enzymes with site-specific scaffold conjugation validate the model and the predicted kinetic enhancements.

Graphical Abstract

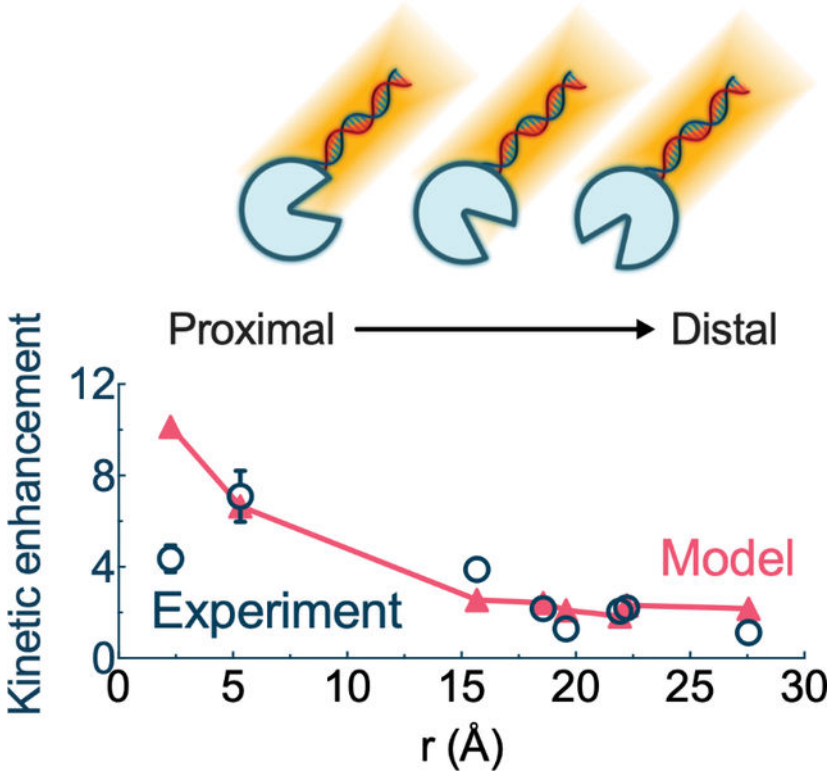

Introduction

A successful strategy to enhance enzyme catalysis is conjugation to a biological or synthetic polymer. Typically, these approaches work to maintain a microenvironment around the enzyme that is favorable to activity and stabilizes an active enzyme structure, thus enabling catalysis at elevated temperatures, in extreme pH, or in non-aqueous solvents [1–4]. Controlling an enzyme's microenvironment can also enhance reaction kinetics [5–7]. For example, polymers and other modifications that create a charged environment around or near the active site of an enzyme can be used to control substrate specificity through charge-complementarity, attracting substrates with opposite charge and repelling like-charged substrates [8,9]. PEGylation, one of the most common enzyme modifications, is often used to increase *in vivo* circulation times for therapeutic proteins and enzymes by protecting against protease degradation. Increased catalytic turnover has also been observed with PEGylation [10,11], an effect likely due to the creation of a microenvironment favorable to reaction kinetics. Similarly, encapsulation in DNA nanostructures or other charged polymers can enhance enzyme turnover by providing a microenvironment that maintains an optimal pH or solvent conditions favorable to catalysis [12].

In a similar approach, we have pursued conjugation strategies to enhance enzyme catalysis using sequence-defined DNA scaffolds to increase the effective substrate concentration around an enzyme. This strategy exploits substrate-scaffold interactions that create a local environment with a higher substrate concentration than the bulk solution. The result is higher reaction rates than would be achieved if the enzyme was exposed to the lower bulk substrate concentration, an effect that is observable by a decrease in the apparent Michaelis constant ($K_{M,app}$) and a corresponding increase in the second order rate constant (k_{cat}/K_M) of the enzyme-DNA conjugate [13–15]. This strategy of controlling an enzyme's effective substrate concentration is also found in nature, where tethered kinase substrates increase phosphorylation rates and substrate selectivity [16–18]. Synthetic mimics of this strategy that tether redox cofactors in close proximity to their enzyme have also been successful in increasing the turnover of nicotinamide adenine dinucleotide (NAD^+) dependent oxidoreductases [19,20]. Collectively, these and other examples that provide a means of controlling the effective concentration of an enzyme's substrate represent a new approach to engineering enhanced enzyme kinetics.

While engineering stability through conjugation is well understood, design rules explaining how to increase enzyme reaction kinetics above wild type levels using conjugation strategies are lacking. To better understand the molecular mechanisms of these effects and advance conjugation approaches focused on enhancing kinetics, a more fundamental understanding of the relationships between the conjugate chemistry, structure, and enzyme kinetics is needed. Here, we address this lack of knowledge through a combined computational, experimental, and modeling approach (Figure 1), the output of which begins to set design rules on how to bring about an increase in effective substrate concentration in an enzyme-DNA conjugate system, and in doing so, links kinetic enhancements to enzyme-DNA features. We do this in the context of a phosphotriesterase-DNA conjugate system (PTE-DNA) that can catalyze the hydrolysis of organophosphates, including the chemical warfare agents VX and Sarin as well as the insecticide paraoxon, use of which is banned in the US and other countries [21,22].

Experimental techniques alone often lack the resolution to accurately explain and predict the enhancements gained from conjugation. As such, we set out to use molecular simulations to study the PTE-DNA system in greater detail and quantify effects that are difficult to assess experimentally. Specifically, we use a multiscale approach combining atomistic molecular dynamics (MD) and rigid-body Brownian dynamics (BD) simulations to capture detailed intermolecular interactions and investigate the concentration gradient of organophosphates around the DNA scaffolds used to modify PTE. We support the computational studies by experimentally testing the positional effect of a single DNA scaffold on enzyme kinetics, and subsequently combine the simulation and experimental data to develop a mechanistic model of the effects of the DNA scaffolds and the position of the conjugation on catalysis. Our results show that our DNA scaffold modifications to PTE decrease K_M through a combination of increased effective substrate concentration around the DNA and by enlarging the substrate capture radius compared to the unconjugated enzyme.

Results and Discussion

We previously developed an enzyme-DNA conjugation strategy that exploits interactions between a DNA scaffold and the enzyme's substrate to enhance catalysis by decreasing the apparent Michaelis constant, K_M. When appropriately designed, catalytic turnover, k_{cat}, is not affected and the second order rate constant, k_{cat}/K_M is increased via the reduction of K_M. The central hypothesis is that the conjugated DNA acts as a substrate-binding scaffold, transiently tethering the substrate to the enzyme and increasing the effective concentration. When applied to PTE and the hydrolysis of organophosphates, we observed an ~11-fold decrease in K_M; PTE monomers were modified with ~7 DNA scaffolds distributed across the surface and with a nucleic acid sequence known to bind the organophosphate paraoxon with a K_d of ~1.4 μM [13]. We have also produced similar results with the model enzyme HRP and an aldo-keto reductase by conjugating 20 bp DNA scaffolds with μM substrate binding to a series of different HRP substrates and to an NAD^+ cofactor mimic, nicotine mononucleotide or NMN^+ [14,15]. In each case, simulations and experiments show that substrate binding may occur in the major and minor groove of the double stranded DNA and via intercalation between base pairs, and that binding to a given substrate is DNA sequence-dependent [23]. Here, we take a multiscale computational approach to quantify the increase in effective concentration that is possible with such DNA scaffolds. Our approach begins with MD- and BD-analysis of the concentration gradient of organophosphate substrates around a double stranded DNA scaffold. The two substrates are paraoxon, which exhibits low μM binding to DNA, and 2,2-dichlorovinyl dimethyl phosphate (DDVP), which does not bind specifically to DNA (predicted K_d of ~1 mM) [13].

Multiscale simulations predict an increase in effective substrate concentration

To better understand the interactions between DNA scaffolds and an enzyme's substrate, we developed a multiscale modeling approach that captures both molecular interactions in atomistic detail and large-scale substrate concentration gradients. As shown in Figure 2a, our analysis for effective substrate concentration began by first defining 5Å-wide regions around a DNA fragment. These were used to quantify the substrate concentration in each region during simulations. Classical MD simulations were used to calculate effective substrate concentration in the region within 5 Å of the DNA. Detailed intermolecular interactions, including solutes, water molecules, and ions, can be modeled explicitly, and therefore accurately quantify the local substrate concentration while the substrate is near the DNA. When the substrate is further from the DNA, the intermolecular van der Waals (vdW) interactions rapidly approach zero and electrostatic attractions are greatly diminished. At longer distances, the resulting dynamics are largely Brownian motion; therefore, we used BD simulations to calculate the effective substrate concentration for regions beyond 5 Å from the DNA [24]. When compared to most enzymes at physiological pH, the high negative charged density of DNA, ($-40\ e^-$ overall vs. $+1e^-$ for PTE) is significantly more important in providing long-ranged electrostatic steering of substrates [25], as such we focused on modeling the DNA scaffold and not a PTE-DNA complex. This focus on modeling the scaffold and not the conjugate structure also enables a more generalizable model that can be readily extended to other enzyme systems. The BD simulations were carried out at 60 μM to match our experiments; however, using the experimental concentration in MD would

result in an intractably large water box. Therefore, a 16 mM substrate concentration was used, which included 64 substrate molecules in total for the MD simulations. We ran two replicates of each simulation to ensure consistency, but present data from only one set of simulations in the main text (Figure 2). Both data sets are available in the supporting information (Figure S1).

In the first shell modeled by MD, where both electrostatic and vdW forces were represented, paraoxon concentration was higher than that of DDVP and $[S]/[S]_0$ was equal to 3.6 for paraoxon and 1.0 for DDVP (Figure 2b). In more distant shells modeled by BD, both substrates maintained effective concentrations above the bulk (*i.e.*, $[S]/[S]_0$ values greater than 1) that gradually decreased with increasing distance. The marginally higher effective paraoxon concentration in the third and fourth shells suggested a slightly stronger long-ranged electrostatic attraction between DNA and the more polar molecule paraoxon, compared with the attractions between DNA and DDVP. Note that substrate molecules bound to the DNA were not included in the concentration calculations, as such molecules are not available to the enzyme and consequently are not an accurate reflection of the effective concentration. Concentration calculations including the bound molecules are presented in Figure S1 and show an exaggerated increase in concentration within the first shell. We proceed to model the overall effect on K_M in later sections using the effective concentration shown in Figure 2b.

Transient binding, effective concentration, and substrate catalytic accessibility

The effective substrate concentration produced by the conjugated DNA should be reflected in the increased number of substrate molecules available for catalysis. Therefore, we calculated the average residence time of the two substrates (both of which carry an overall neutral charge) on the DNA in the MD trajectories to ensure that substrates are in close proximity to the enzyme and are available for reaction. The residence time was defined as the amount of time for which one substrate molecule was within 4.5 Å of the DNA. Average residence times for paraoxon and DDVP were 208 ps and 86 ps, respectively. The number of distinct substrate-DNA contacts for each substrate was similar, meaning a roughly equal number of DDVP and paraoxon molecules encountered the DNA, but paraoxon stayed bound to DNA for 2.4 times longer.

In addition to the residence time calculations, we also explored the binding modes of each substrate to gain mechanistic insights into intermolecular attractions. We observed that paraoxon bound in the DNA minor groove as well as to the terminal DNA bases through pi-stacking interactions, and at least one paraoxon molecule bound to the major groove before intercalating between two base pairs (Figure S2). The intercalated molecule formed a stable interaction that lasted ~70 ns, the longest interaction observed in any of our simulations. DDVP interactions with DNA were shorter-lived and electrostatic in nature, primarily taking place near the highly polar backbone and at the ends of the DNA strand. Overall, the average residence times of both substrates were tens to hundreds of picoseconds, much shorter than the catalytic rate of PTE, which is on the order of 2000 s^{-1} (see refs. [13,26]). Taken together, these simulations are highly supportive of our central hypothesis that a rationally designed DNA sequence with micromolar binding to a substrate of interest can increase the effective

concentration near the conjugated scaffold, and importantly, increase the available substrate molecules for catalysis.

Azido side chain amino acid incorporation enables site specific bioconjugation of DNA scaffolds

Given that our simulations predicted that the local concentration of paraoxon is significantly increased within a few nm of the DNA scaffold, we sought to test the positional effect of the scaffold on catalysis and determine the distance from the active site when catalysis can be enhanced. To do so, we used non-canonical amino acid technology to create a series of PTE mutants that enabled the bioconjugation of a DNA fragment at defined distances from the active site. Specifically, DNA modified with dibenzocyclooctyl (DBCO) was reacted with the azido side chain of p-azido-phenylalanine (pAzf) [27]. Residue positions D133, K175, F149, A78, K294, T352, D160, and A364 were modified to create a series of eight unique PTE-DNA constructs each with a different distance between the attached DNA to the active site. The mutant positions and distance from DNA to active site, measured based on the 1HZY PDB structure of PTE, are D133 (2.3 Å), K175 (5.3 Å), F149 (15.7 Å), A78 (19.6 Å), K294 (20.1 Å), T352 (22.0 Å), D160 (22.1 Å), and A364 (27.6 Å).

Confirmation that a single DNA scaffold was attached to a PTE mutant is shown in Figure S3. A 260 nm spectral peak proportional to the amount of attached DNA is observed with conjugation to PTE (see Supporting Information (SI): Experimental Methods), and analysis of PTE-DNA K175pAzF revealed that on average 1.1±0.1 DNA fragments were attached to each PTE monomer using the click chemistry approach (note, PTE is a functional dimer). In comparison, when DNA is conjugated to PTE at every accessible lysine side chain via bifunctional sulfo-NHS-ester/maleimide chemistry to thiolated DNA fragments, 7.2±0.7 scaffolds were attached per monomer. This construct, PTE-DNA_7, includes DNA scaffolds that are conjugated to PTE at distances that overlap with the range of the distances of the singly modified constructs created in this work.

The Michaelis constant, K_M, reaches a minimum in close proximity to the enzyme active site

With the series of PTE-DNA constructs in-hand, we set out to characterize the effect of DNA position on enzyme kinetics. Figure 3 presents both the kinetic analysis of each mutant as well as an image of the crystal structure of PTE with the position of the active site and incorporated pAzf amino acid indicated; the kinetic curves and images are arranged according to the distance between conjugated DNA and the active site increasing in distance from the top left to the bottom right with the PTE-DNA_7 control construct as the last entry of the figure. PTE-DNA_7 is notable because the turnover rate (k_{cat}) is unchanged in comparison to unmodified PTE (Table 1). Similarly, the k_{cat} values of the PTE-DNA constructs are relatively unchanged in comparison to unmodified PTE; only mutations to positions 133, 160, and 352 resulted in a significant decrease in k_{cat}. In the case of position 133, turnover with and without attached DNA was substantially reduced in comparison to PTE, likely because the active site was altered with the incorporation of pAzf. Incorporation at positions 160 and 352 also decreased k_{cat}, but in these cases the reduction was limited to ~10% or less. Given this, we focused on the effect of DNA position on K_M using the

series of mutants that established a distance range between the DNA scaffold attachment site and the enzyme's active site of 5.3 to 27.6 Å (see SI Methods for details of the distance calculations). The kinetic effect of DNA conjugation position can be visually seen in the series of kinetic curves for the PTE-DNA complexes (Figure 3). When the DNA is attached far from the active site (*i.e.*, A364pAzf; 27.6 Å) the kinetic curves and parameters (k_{cat} and K_M) of the modified and unmodified PTE mutants are identical. As the distance between the DNA scaffold and the active site decreases, the PTE-DNA kinetic curve shifts leftward, rates at lower substrate concentrations are increased, and the K_M parameter is reduced. At 5.3 Å distance (attachment at position 175), K_M is reduced by 7.1-fold, an enhancement that is well-matched with that achieved with PTE-DNA$_7$, which contains a scaffold at the same position. At longer distances, a reduction in K_M was also observed: at 15.7 Å (position 149), the DNA scaffold reduced K_M by 4.4-fold; at distances between 19.6 and 22.1 Å (positions 78, 160, and 352) the enhancement ranged between 2.1- and 2.2-fold. One exception in this range is position 294, which is 20.1 Å from the active site; conjugation here only decreased K_M by ~30%. Lastly, at 27.6 Å (position 364) the enhancement was not statistically significant.

To verify that the enhancement in K_M was a result of the paraoxon-DNA interactions and the predicted increase in effective concentration that resulted from these interactions, we repeated the kinetic analysis with the non-binding control substrate DDVP (Figure S4 and Table S1). Mutation to D133, the closest conjugation site at 2.3 Å distance, was again detrimental on kinetics, but the effect with DDVP as a substrate was more pronounced in K_M, which increased 5-fold in the presence of a DNA scaffold. Attachment to the K175pAzF mutant, which is 5.3 Å from the active site and enhanced paraoxon binding by 7.1-fold, did not have an effect on the hydrolysis of DDVP, likely due to the lack of DDVP-DNA interactions and absence of an increased effective substrate concentration. As expected, conjugation to position 364 showed no significant changes in reaction kinetics with DDVP or with paraoxon, as the conjugation position is too far from the active site to affect the local substrate concentration. Additional evidence for the increased effective concentration effect on PTE kinetics was acquired through a series of activity assays with increasing viscosity. When enzyme activity is wholly or partially diffusion limited, such assays can be used to determine the substrate on-rate, k_1 [13,15,28]. This on-rate analysis revealed that decreases in K_M due to the attachment of a DNA scaffold were accompanied by an increase in paraoxon on-rate, and that in the absence of a change in K_M, DDVP and paraoxon on-rates were unchanged in comparison to unmodified PTE (Figure S4).

Modeling the substrate capture radius enables prediction of K_M enhancements

To help render our kinetic analyses into a more fundamental understanding of how the position of a conjugated scaffold can affect enzyme catalysis, we set out to develop a biophysical model to predict the fold enhancement of K_M achieved for any conjugation site. The model begins with a definition of K_M, where K_M is inversely proportional to the enzyme-substrate association rate, k_{on}, and can be expressed as

$$K_M = \frac{k_{off} + k_{cat}}{k_{on}} \quad (1)$$

Where k_{cat} is the catalytic turnover rate, k_{off} is the rate of dissociation, and k_{on} is the substrate association rate. Since turnover is largely unaffected by conjugation of the DNA scaffold (see Table 1), we make the assumption that k_{off} is also unchanged. Given this, changes in K_M are dependent on k_{on} (or k_1), and a model that captures changes to the on-rate should enable the prediction of K_M after conjugation ($K_{M,app}$). The multiscale simulations (Figure 2) and kinetic analysis of PTE-DNA constructs with various conjugation sites suggest a direct proportionality between the effective substrate concentration, $[S]/[S]_0$, and the enhancement in K_M, which can be expressed as

$$\frac{K_M}{K_{M,app}} \propto \frac{[S]}{[S]_0} \tag{2}$$

Such a relationship is also observed when enzymes are immobilized on a charged support that creates a substrate concentration gradient from the bulk to the surface [29]. While this intuitive relationship is observed with our simulation data, it is not the only factor contributing to the enhancement in K_M. This can be seen in Figure 4, in which the curve representing the effective concentration lags behind the experimentally measured K_M enhancements. The physical presence of the attached DNA scaffold is also likely to contribute to the effect as it can act as an extension of the enzyme, increasing the substrate capture radius of the PTE-DNA complex relative to unmodified PTE. The standard kinetic theory for collisions per unit time, α, between to molecules experiencing attractive intermolecular forces is

$$\alpha = \frac{4\pi CD}{\int_{r_0}^{\infty} \frac{1}{r^2} e^{\frac{-U(r)}{kT}}} = 4\pi CDr^* \tag{3}$$

The collision rate depends on C, the substrate concentration; D, the relative diffusion coefficient of the molecules; and the length r, the sum of the radii of the two molecules. The radius r* is the larger effective radius after accounting for intermolecular attraction [30,31]. Here, we model the effect of DNA conjugation as an increase in r* since the DNA strand acts as a lure for substrate both energetically and sterically. The energetic contribution to the molecular collision rate is already accounted for in the substrate distribution quantified by the simulations; that is, it can be thought of as an increase in C in equation (3). Next, we can relate the ratio of the capture radius of the DNA-modified enzyme to that of the unmodified enzyme as

$$\frac{r_{PTE} + DNA}{r_{PTE}} \tag{4}$$

where r_{PTE} is the radius of gyration of the PTE enzyme and $r_{PTE+DNA}$ is the sum of r_{PTE} and r_{DNA}. Since the DNA is a very elongated molecule, equation (5) can be used to estimate its effective radius r_{DNA} as

$$r_{DNA} = \frac{a}{ln\frac{2a}{b}} \quad (5)$$

where a and b are the major and minor semiaxes [31]. However, simply accounting for the linear extension of the DNA is not adequate. As the conjugation site becomes more distant from the enzyme active site, the angle between DNA and the active site grows, and the efficiency of substrate shuttling to the active site diminishes. This "offset angle" (θ_{DNA}) is defined as the angle between a vector from the enzyme center to the active site catalytic residues and a vector from the enzyme center to the conjugation site (Figure S5). The overall effect of the conjugated DNA, γ, is then modeled as

$$\gamma = 1 + \left[\frac{\pi - \theta_{DNA}}{\pi}\left(\frac{r_{PTE+DNA}}{r_{PTE}} - 1\right)\right] \quad (6)$$

In the parameter γ, θ_{DNA} is allowed to cover the range of π radians, or 180 degrees. When θ_{DNA} is 0, the enlargement of the active site due to DNA conjugation can be fully exploited. When θ_{DNA} is π radians, the effective extension from DNA conjugation is zero since the DNA is too far from the active site to increase the flow of substrate there. Altogether, the fold decrease in K_M can then be predicted as

$$\frac{K_M}{K_{M,app}} = \frac{[S]}{[S]_0}\gamma \quad (7)$$

As shown in Figure 4, the substrate-capture window model described by equations (6) and (7) is in good agreement with our experiments and yields an obvious improvement over measurement of $[S]/[S]_0$ alone (see SI and Figure S6 for example calculations and full details). The model matches the non-linear increase in K_M enhancement when the distance between the scaffold conjugation site and the active site is less than ~20 Å. There is also good agreement with the experimental results at longer distances, suggesting that the combination of distance- and angle-dependence is needed to explain the effect, and that the substrate concentration around the scaffold alone is insufficient to explain the observed experimental results. One exception to this trend is position 294, which resulted in only a minimal decrease in K_M while other positions at similar distances resulted in ~2-fold enhancement. We recognize that enzyme surfaces may possess energetic channels that efficiently shuttle substrates to the active site *via* surface diffusion. Conversely, they may possess attractive regions that sequester substrate, preventing diffusion to the active site. Both of these effects could explain deviations from the model as they are not explicitly accounted for. We also note that the largest discrepancy between the model and experiment occurs with modification at position D133. Conjugation here significantly disrupted catalytic activity, likely due to blocking of the active site due to the presence of the DNA, which was only 2.3 Å from the opening of the active site (Figure S7). With a radius of 8–10 Å (small axis), DNA overlapped considerably with the catalytic site (Figure S8). We also note that the incorporation of pAzF in this position decreased kinetics.

Overall, these results show that the K_M enhancement is not entirely explained by local substrate concentration increase, and that structural features of the conjugated complex also play a role. Our model demonstrates this effect by taking into account three structural features encapsulated in the parameter γ. These include the size of the enzyme, size of the scaffold (in our case a 20 bp DNA fragment), and the attachment position, all of which can be determined given a crystal structure (or accurate homology model) of the enzyme, an approximate model of the scaffold structure, and knowledge of the conjugation site. The second critical parameter is the effective substrate concentration ($[S]/[S]_o$), which is a function of the strength of the substrate-scaffold interactions. Here, we use a multiscale approach that is suitable for many other substrates and scaffolds. Alternatively, solely BD-based or other modeling approaches could potentially be used to generate a reasonable approximation of $[S]/[S]_o$ as a function of distance from the selected scaffold. Using the PTE-DNA systems as an example, we show how experimental analyses combined with simple computational techniques can help explain and predict catalytic enhancement in enzyme-scaffold conjugates.

Enzyme activity can be enhanced through a wide range of bioconjugation strategies that create enzyme-scaffold complexes with controlled microenvironments. In this work, we show that computationally guided enzyme-scaffold design can result in predictable enhancements in an enzyme's Michaelis constant, K_M, and increase the second order rate constant k_{cat}/K_M. A rationally designed DNA covalently attached to the enzyme PTE attracts the desired substrate (paraoxon) increasing the effective substrate concentration around the enzyme, an effect that results in a substantial decrease in K_M, an increase in substrate on-rate, k_1, and maintains the high catalytic turnover of the unmodified enzyme. The multiscale simulations combining MD and BD simulations showed that the increase in substrate concentration near the DNA scaffold is due to both electrostatic attraction and short-range vdW forces and allowed the concentration gradient around the scaffold to be quantified. Using site selective conjugation, we created a series of PTE-DNA complexes that differ in the distance and angle between conjugated DNA scaffold and the enzyme's active site, and in doing so were able to experimentally determine the effect of scaffold position on enzyme kinetics. Based on the experimental and computational results, we develop a model that predicts K_M enhancements based on the position of the conjugated scaffold; conjugation in close proximity to the active site without sterically blocking access achieved the greatest enhancement in enzyme kinetics, a 7.1-fold decrease in K_M. The model, along with the experimental and computational results, represent a new design approach to enhancing enzyme catalysis through controlled microenvironments where conjugated scaffolds are used to increase the effective substrate concentration of an enzyme. While this work and the resulting design principles were developed using PTE modified with a DNA scaffold, we anticipate that this approach can be used to design enhanced catalysis with other enzyme-scaffold bioconjugates, of which there are many examples that have binding properties to substrates of interest.

Experimental Procedures

Resource Availability

Lead Contact—Further information and requests for resources and reagents should be directed to and will be fulfilled by the Lead Contact, Ian Wheeldon (wheeldon@ucr.edu).

Materials Availability—No new reagents are synthesized in this study.

Data and Code Availability—This study did not generate/analyze datasets/code.

Materials and Methods

See Supporting Information for Computational and Experimental Materials and Methods, including molecular dynamics simulations; brownian dynamics simulations; radial distribution of paraoxon and DDVP around DNA; calculation of paraoxon and DDVP residence time on DNA, and experimental methods including PTE cloning, expression and purification; incorporation of, and click-chemistry with p-azido-phenylalanine (pAzF); PTE-DNA conjugation by bifunctional sulfo-NHS-ester/maleimide chemistry; UV-vis analysis of PTE:DNA complexes; PTE and PTE-DNA kinetic analysis; Electrophoretic analysis of pAzf incorporation into PTE; calculation of model parameters; and example calculation of predicted K_M enhancement.

Supplementary Material

Refer to Web version on PubMed Central for supplementary material.

Acknowledgements and funding sources

This study was supported by Army Research Office MURI grant W911NF1410263, the US National Science Foundation grant MCB-1932984 and US National Institutes of Health grant GM-109045.

References

1. Yan M, Ge J, Liu Z, and Ouyang P (2006). Encapsulation of single enzyme in nanogel with enhanced biocatalytic activity and stability. J. Am. Chem. Soc. 128, 11008–11009. [PubMed: 16925402]
2. Zhang P, Sun F, Tsao C, Liu S, Jain P, Sinclair A, Hung H-C, Bai T, Wu K, and Jiang S (2015). Zwitterionic gel encapsulation promotes protein stability, enhances pharmacokinetics, and reduces immunogenicity. Proc. Natl. Acad. Sci. U. S. A. 112, 12046–12051. [PubMed: 26371311]
3. Zaks A, and Klibanov A (1984). Enzymatic catalysis in organic media at 100 degrees C. Science 224, 1249–1251. [PubMed: 6729453]
4. Chapman R, and Stenzel MH (2019). All Wrapped up: Stabilization of Enzymes within Single Enzyme Nanoparticles. J. Am. Chem. Soc. 141, 2754–2769. [PubMed: 30621398]
5. Zhang Y, Ge J, and Liu Z (2015). Enhanced Activity of Immobilized or Chemically Modified Enzymes. ACS Catalysis 5, 4503–4513.
6. Lancaster L, Abdallah W, Banta S, and Wheeldon I (2018). Engineering enzyme microenvironments for enhanced biocatalysis. Chem. Soc. Rev. 47, 5177–5186. [PubMed: 29796541]
7. Huber GA, and McCammon JA (2019). Brownian Dynamics Simulations of Biological Molecules. Trends Chem 1, 727–738. [PubMed: 32309795]
8. Azuma Y, Bader DLV, and Hilvert D (2018). Substrate Sorting by a Supercharged Nanoreactor. J. Am. Chem. Soc. 140, 860–863. [PubMed: 29278496]

9. Kraj P, Selivanovitch E, Lee B, and Douglas T (2021). Polymer Coatings on Virus-like Particle Nanoreactors at Low Ionic Strength-Charge Reversal and Substrate Access. Biomacromolecules 22, 2107–2118. [PubMed: 33877799]
10. Daffu GK, Lopez P, Katz F, Vinogradov M, Zhan C-G, Landry DW, and Macdonald J (2015). Sulfhydryl-specific PEGylation of phosphotriesterase cysteine mutants for organophosphate detoxification. Protein Eng. Des. Sel. 28, 501–506. [PubMed: 26243887]
11. Efremenko EN, Lyagin IV, Klyachko NL, Bronich T, Zavyalova NV, Jiang Y, and Kabanov AV (2017). A simple and highly effective catalytic nanozyme scavenger for organophosphorus neurotoxins. J. Control. Release 247, 175–181. [PubMed: 28043864]
12. Zhang Y, Wang Q, and Hess H (2017). Increasing Enzyme Cascade Throughput by pH-Engineering the Microenvironment of Individual Enzymes. ACS Catalysis 7, 2047–2051.
13. Lang X, Hong X, Baker CA, Otto TC, and Wheeldon I (2020). Molecular binding scaffolds increase local substrate concentration enhancing the enzymatic hydrolysis of VX nerve agent. Biotechnol. Bioeng. 117, 1970–1978. [PubMed: 32239488]
14. Gao Y, Roberts CC, Zhu J, Lin J-L, Chang C-EA, and Wheeldon I (2015). Tuning Enzyme Kinetics through Designed Intermolecular Interactions Far from the Active Site. ACS Catalysis 5, 2149–2153.
15. Gao Y, Roberts CC, Toop A, Chang C-EA, and Wheeldon I (2016). Mechanisms of Enhanced Catalysis in Enzyme-DNA Nanostructures Revealed through Molecular Simulations and Experimental Analysis. Chembiochem 17, 1430–1436. [PubMed: 27173175]
16. Dyla M, and Kjaergaard M (2020). Intrinsically disordered linkers control tethered kinases via effective concentration. Proc. Natl. Acad. Sci. U. S. A. 117, 21413–21419. [PubMed: 32817491]
17. Siddiqui JK, Tikunova SB, Walton SD, Liu B, Meyer M, de Tombe PP, Neilson N, Kekenes-Huskey PM, Salhi HE, Janssen PML, et al. (2016). Myofilament Calcium Sensitivity: Consequences of the Effective Concentration of Troponin I. Front. Physiol. 0.
18. Cool AM, and Lindert S (2021). Computational Methods Elucidate Consequences of Mutations and Post-translational Modifications on Troponin I Effective Concentration to Troponin C. J. Phys. Chem. B 125.
19. Fu J, Yang YR, Johnson-Buck A, Liu M, Liu Y, Walter NG, Woodbury NW, and Yan H (2014). Multi-enzyme complexes on DNA scaffolds capable of substrate channelling with an artificial swinging arm. Nat. Nanotechnol. 9, 531–536. [PubMed: 24859813]
20. Ozbakir HF, Garcia KE, and Banta S (2018). Creation of a formate: malate oxidoreductase by fusion of dehydrogenase enzymes with PEGylated cofactor swing arms. Protein Eng. Des. Sel. 31, 103–108. [PubMed: 29660073]
21. Olsvik PA, and Søfteland L (2020). Mixture toxicity of chlorpyrifos-methyl, pirimiphos-methyl, and nonylphenol in Atlantic salmon () hepatocytes. Toxicol Rep 7, 547–558. [PubMed: 32373476]
22. Laetz CA, Baldwin DH, Hebert V, Stark JD, and Scholz NL (2013). Interactive neurobehavioral toxicity of diazinon, malathion, and ethoprop to juvenile coho salmon. Environ. Sci. Technol. 47, 2925–2931. [PubMed: 23409965]
23. Lang X, Zhu L, Gao Y, and Wheeldon I (2017). Enhancing Enzyme Activity and Immobilization in Nanostructured Inorganic–Enzyme Complexes. Langmuir 33, 9073–9080. [PubMed: 28813159]
24. Votapka LW, and Amaro RE (2015). Multiscale Estimation of Binding Kinetics Using Brownian Dynamics, Molecular Dynamics and Milestoning. PLoS Comput. Biol. 11, e1004381. [PubMed: 26505480]
25. Breger JC, Ancona MG, Walper SA, Oh E, Susumu K, Stewart MH, Deschamps JR, and Medintz IL (2015). Understanding How Nanoparticle Attachment Enhances Phosphotriesterase Kinetic Efficiency. ACS Nano 9, 8491–8503. [PubMed: 26230391]
26. Roodveldt C, and Tawfik DS (2005). Directed evolution of phosphotriesterase from Pseudomonas diminuta for heterologous expression in Escherichia coli results in stabilization of the metal-free state. Protein Eng. Des. Sel. 18, 51–58. [PubMed: 15790580]
27. Chin JW, Santoro SW, Martin AB, King DS, Wang L, and Schultz PG (2002). Addition of p-azido-L-phenylalanine to the genetic code of Escherichia coli. J. Am. Chem. Soc. 124, 9026–9027. [PubMed: 12148987]

28. Brouwer AC, and Kirsch JF (1982). Investigation of diffusion-limited rates of chymotrypsin reactions by viscosity variation. Biochemistry 21, 1302–1307. [PubMed: 7074086]

29. Clark DS, and Blanch HW (1997). Biochemical Engineering (CRC Press).

30. Jackson MB (2010). Molecular and Cellular Biophysics (Cambridge University Press).

31. Berg OG, and von Hippel PH (1985). Diffusion-controlled macromolecular interactions. Annu. Rev. Biophys. Biophys. Chem. 14, 131–160. [PubMed: 3890878]

Bigger Picture

Conjugation of molecular scaffolds to enzymes has begun to replace enzyme immobilization on solid supports. These new DNA, protein, and polymer scaffolds can provide nanoscale-level precision in terms of their chemistry and physical structure and are used to create stable enzyme particles of a desired size, shape, and activity. Here, we use multiscale modeling and experiments to define design rules for the creation of enzyme-DNA complexes with enhanced kinetics. We show that changes in an enzyme's chemical and physical microenvironment created by the conjugated DNA can alter enzyme kinetics in a controllable manner. In doing so, we show that conjugation position should be given as much attention in enzyme engineering as the chemistry and structure of the scaffold itself.

Highlights

1. Predictive design of enhanced kinetics in DNA modified phosphotriesterase
2. Multiscale simulations quantify the effective substrate concentration around DNA
3. Site selective scaffold conjugation validates predictive model outputs.

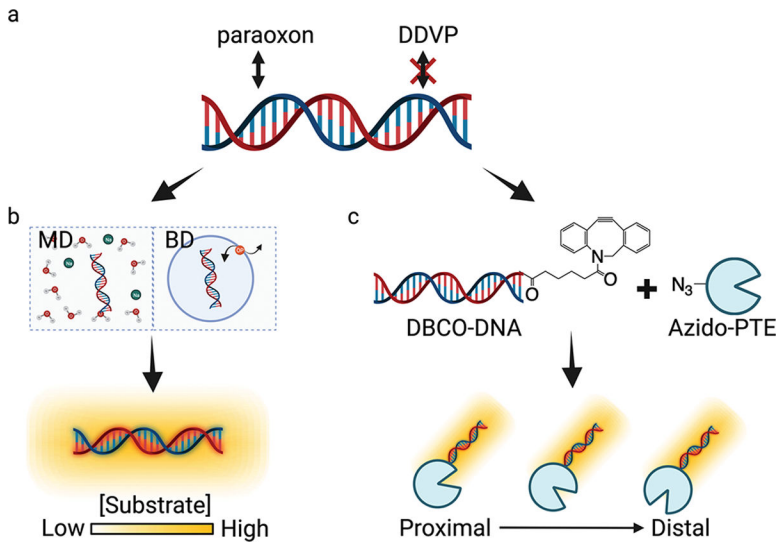

Figure 1. A multiscale computational and experimental approach to understanding the positional effects of DNA scaffolds on enzyme kinetics.

(a) Rationally designed DNA scaffolds can bind the organophosphates in a sequence-dependent manner. Paraoxon, the model compound used here, binds with low μM affinity, while 2,2-dichlorovinyl dimethyl phosphate (DDVP) does not interact strongly with DNA. (b) Multiscale simulations are used to predict the effective substrate concentration around a DNA scaffold. MD refers to molecular dynamic simulations, while BD refers to Brownian dynamic simulations. (c) Non-natural amino acid chemistry is used to position DNA scaffolds at defined positions on the enzyme phosphotriesterase (PTE). Conjugation by click chemistry is facilitated by dibenzocyclooctyl (DBCO) modified DNA and the azido side chain of an incorporated p-azido-phenylalanine (pAzF) residue.

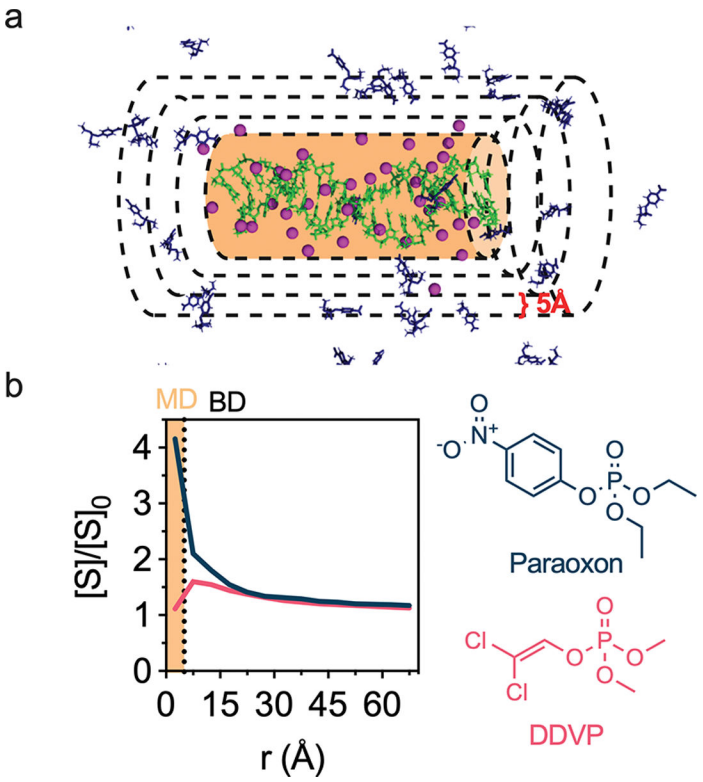

Figure 2. Multiscale modeling of the effective concentration around DNA scaffolds.

(**a**) A screenshot of a molecular dynamics simulation featuring paraoxon (dark blue) around a length of double-stranded DNA containing salt (purple). The effective substrate concentration in concentric shells enclosing the DNA (green) was calculated by averaging substrate concentrations in 5 Å thick cylindrical shell across the simulation time. The shells extend outward from the DNA to 100 Å; only the first four shells are depicted here for clarity. The concentration up to 5 Å from DNA (yellow shell) was quantified using MD simulations; the concentration beyond 5 Å was quantified using BD simulations. (**b**) Paraoxon and DDVP effective concentration curves after combining MD data from the first shell with BD data for all other shells.

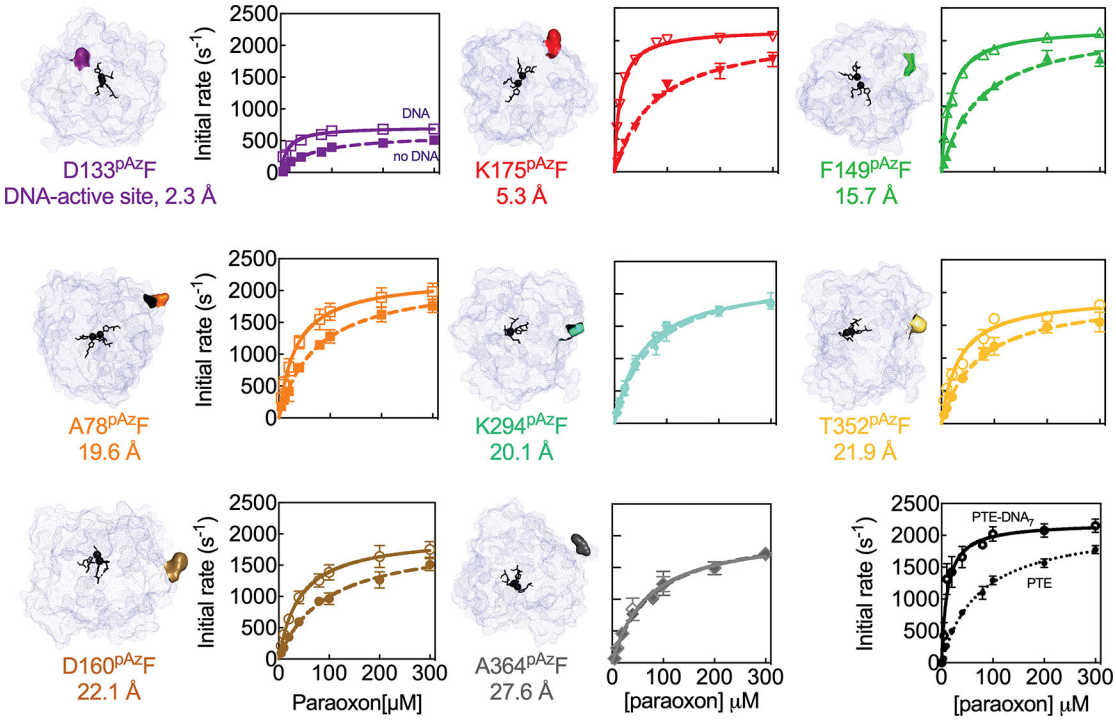

Figure 3. The effect of DNA position on PTE kinetics.

Kinetic analysis and the crystal structure of PTE is shown for each PTE^{pAzF} mutant with (solid line) and without (dashed line) the conjugation of one or more DNA scaffolds. The image of each crystal structure (gray mesh) has been modified to show the position of pAzF incorporation (colored residues) and the active site (black with residue side chains shown). Distance between the conjugation and active sites is stated for each mutant. DNA fragments are not shown for clarity. (Bottom, Right) PTE and PTE modified with ~7 DNA scaffolds per PTE monomer conjugated to free lysine groups by NHS-conjugation chemistry is shown as a comparison to the single DNA modifications achieved with the site-specific incorporation of pAzF.

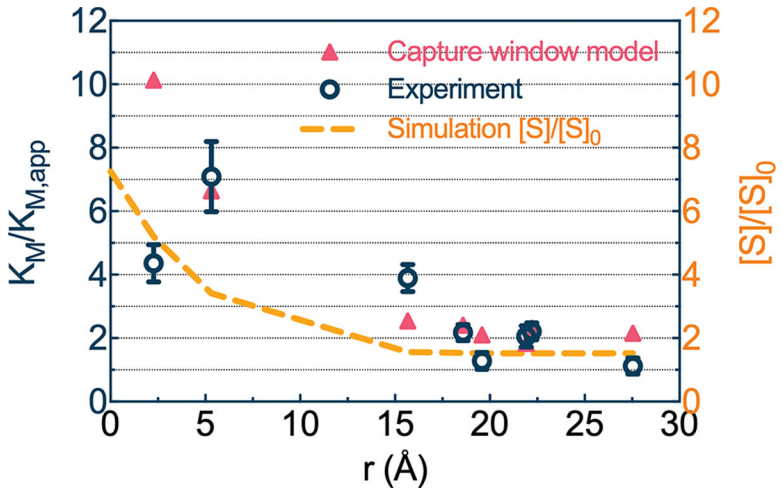

Figure 4. Mechanistic modeling captures the position-dependent kinetic enhancements of PTE-DNA conjugates.

Left y-axis: Experimental (circle) and model predicted (triangle) of K_M enhancement for paraoxon hydrolysis by DNA modified PTE. Right y-axis: Effective substrate concentration, $[S]/[S]_0$, predicted by multiscale simulations.

Table 1.

Kinetic parameters of PTE-DNA and PTE mutants.

PTE Mutants	Distance (Å)	PTE				PTE-DNA$_1$			
		k_{cat} (s^{-1})		K_M (μM)		k_{cat} (s^{-1})		$K_{M,app}$ (μM)	
D133pAzF	2.3	612±39	****	61±10	ns	730±38	****	14±3	****
K175pAzF	5.3	2175±120	ns	78±12	ns	2180±35	ns	11±3	****
F149pAzF	15.7	2030±120	ns	74±14	ns	2110±58	ns	19±2	****
A78pAzF	19.6	2210±143	ns	74±12	ns	2210±117	ns	34±6	****
K294pAzF	20.1	2140±172	ns	71±14	ns	2240±113	ns	55±10	***
T352pAzF	22.0	1950±146	**	70±13	ns	1963±164	**	34±9	****
D160pAzF	22.1	1990±143	*	93±16	*	1980±110	**	42±7	****
A364pAzF	27.6	2350±163	ns	78±15	ns	2070±151	ns	69±13	ns
PTE	-	2185±122		73±10		-		-	
PTE-DNA$_7$	-	-		-		2198±143		11±3.1	

Statistical significance in comparison to PTE in the absence of DNA conjugation is stated with “ns” indicating a p value> 0.05 (not significant)

* is 0.01≤p<0.05

** 0.001≤p<0.01

*** is 0.0001≤p<0.001, and

**** is p<0.0001.

Data are mean ± standard deviation.